Diffusion-weighted imaging of the prostate: image quality and geometric distortion of readout-segmented versus selective-excitation accelerated acquisitions

Barth, Borna K ; Cornelius, Alexander ; Nanz, Daniel ; Eberli, Daniel ; Donati, Olivio F

Abstract: OBJECTIVE: To compare image quality and geometric distortion between readout-segmented diffusion-weighted imaging (rs-DWI) and selective-excitation accelerated reduced-field of view (FOV) DWI (sTX-DWI) of the prostate. MATERIALS AND METHODS: Sixty-five patients underwent 3-T MRI of the prostate including rs-DWI and sTX-DWI (b values, 0, 50, and 1000 seconds/mm; FOV, 150 × 150 mm and 77 ×150 mm for rs-DWI and sTX-DWI; slice thickness, 3 mm; acquisition time, 8:18 min and 1:37 min for rs-DWI and sTX-DWI). Two readers evaluated aspects of image quality and geometric distortion on a 5-point Likert scale. Quantitative analysis of geometric distortion was assessed by measurements of anteroposterior and left-right diameters and compared to T2-weighted turbo-spin echo sequence using intraclass correlation coefficient (ICC). RESULTS: There was no significant difference in resolution, capsule demarcation, and zonal anatomy (P = 0.111-0.866). Overall image quality was rated "above average" by reader 1 (4.09 ± 0.66 and 4.03 ± 0.79; P = 0.433) and reader 2 (3.86 ± 0.66 and 3.80 ± 0.74; P = 0.465) for rs-DWI and sTX-DWI. Reader 1 (0.74 ± 0.67 and 1.17 ± 0.84; P < 0.001) and reader 2 (0.55 ± 0.64 and 1.09 ± 0.95; P < 0.001) rated the level of geometric distortion significantly lower for rs-DWI than sTX-DWI. Readout-segmented DWI (0.9 ± 2.2 mm) and sTX-DWI (2.1 ± 3.8 mm) overestimated the anteroposterior diameter of the prostate compared to T2-weighted turbo-spin echo sequence (P < 0.001), the difference being more pronounced for sTX-DWI [ICC, 0.89 (95% confidence interval, 0.83-0.93)] compared to rs-DWI [ICC, 0.96 (95% confidence interval, 0.94-0.96)]. CONCLUSION: Selective-excitation accelerated reduced-FOV DW images (sTX-DWI) of the prostate can be acquired more than 5 times faster than rs-DWI with comparable image quality, at the expense of significantly increased geometric distortion.

DOI: https://doi.org/10.1097/RLI.0000000000000184

Diffusion-Weighted Imaging of the Prostate

Image Quality and Geometric Distortion of Readout-Segmented Versus Selective-Excitation Accelerated Acquisitions

Borna K. Barth, MD, Alexander Cornelius, MD,† Daniel Nanz, PhD,* Daniel Eberli, MD, PhD,‡ and Olivio F. Donati, MD**

Objective: To compare image quality and geometric distortion between readout-segmented diffusion-weighted imaging (rs-DWI) and selective-excitation accelerated reduced-field of view (FOV) DWI (sTX-DWI) of the prostate.

Materials and Methods: Sixty-five patients underwent 3-T MRI of the prostate including rs-DWI and sTX-DWI (b values, 0, 50, and 1000 seconds/mm^2; FOV, 150 × 150 mm^2 and 77 ×150 mm^2 for rs-DWI and sTX-DWI; slice thickness, 3 mm; acquisition time, 8:18 min and 1:37 min for rs-DWI and sTX-DWI). Two readers evaluated aspects of image quality and geometric distortion on a 5-point Likert scale. Quantitative analysis of geometric distortion was assessed by measurements of anteroposterior and left-right diameters and compared to T2-weighted turbo-spin echo sequence using intraclass correlation coefficient (ICC).

Results: There was no significant difference in resolution, capsule demarcation, and zonal anatomy (P = 0.111–0.866). Overall image quality was rated "above average" by reader 1 (4.09 ± 0.66 and 4.03 ± 0.79; P = 0.433) and reader 2 (3.86 ± 0.66 and 3.80 ± 0.74; P = 0.465) for rs-DWI and sTX-DWI. Reader 1 (0.74 ± 0.67 and 1.17 ± 0.84; P < 0.001) and reader 2 (0.55 ± 0.64 and 1.09 ± 0.95; P < 0.001) rated the level of geometric distortion significantly lower for rs-DWI than sTX-DWI.

Readout-segmented DWI (0.9 ± 2.2 mm) and sTX-DWI (2.1 ± 3.8 mm) overestimated the anteroposterior diameter of the prostate compared to T2-weighted turbo-spin echo sequence (P < 0.001), the difference being more pronounced for sTX-DWI [ICC, 0.89 (95% confidence interval, 0.83-0.93)] compared to rs-DWI [ICC, 0.96 (95% confidence interval, 0.94–0.96)].

Conclusion: Selective-excitation accelerated reduced-FOV DW images (sTX-DWI) of the prostate can be acquired more than 5 times faster than rs-DWI with comparable image quality, at the expense of significantly increased geometric distortion.

Key Words: diffusion-weighted imaging, magnetic resonance imaging, prostate, read out segmented, reduced field of view

(*Invest Radiol* 2015;00: 00–00)

Diffusion-weighted imaging (DWI) is an integral component of multiparametric magnetic resonance imaging (MRI) (mpMRI) of the prostate,[1–3] improving diagnostic performance in cancer detection and assessment of cancer aggressiveness.[4–9] Although the use of echoplanar imaging has enabled high-quality DWI, some challenges remain, such as geometric distortion or susceptibility artifacts as a result of inhomogeneities of the static magnetic field. These are more pronounced at higher field strengths often used in prostate MRI.[1,10] One recently introduced technique addresses the issue of geometric distortion and susceptibility artifacts by dividing the k-space trajectory into multiple segments in the readout direction, that is, by a readout-segmented echoplanar imaging sequence (rs-DWI),[11] which has previously been used in intracranial[12–14] and pelvic imaging.[15] The latter sequence can achieve higher image resolution and a reduction of susceptibility-based artifacts due to a shorter echo spacing and a shorter echo-train segment length compared to the traditional single-shot echoplanar sequence (ss-DWI), which is currently the most widely used sequence for mpMRI of the prostate.[11] However, the potentially superior image quality is typically achieved at the cost of a prolonged scan time.[16]

Another technical advancement in DWI sequences leading to a reduction of artifacts related to B0 and B1 inhomogeneity has been introduced recently. With dynamic parallel transmit-based selective-excitation technology (sTX), radiofrequency waveforms and gradient amplitudes can be individually modulated within a 2- or 3-channel radiofrequency transmitter so as to control magnitude and phase of the RF pulse allowing for patient- and volume-specific B1-shimming and therefore leading to a more homogeneous excitation within the field-of-view (FOV).[17] The second hallmark of dynamic sTX is the possibility to selectively excite a defined volume, allowing for a reduction of the FOV in phase-encoding direction and thereby accelerating acquisition time while maintaining spatial resolution.[17] Due to in-plane selective excitation, the FOV along the phase-encoding direction does not need to cover the whole anatomy to avoid aliasing or wrap-around artifacts; thus, the minimum number of phase-encoding steps is reduced, which may be used to shorten the scan time. Whereas both sequence types, sTX-DWI and rs-DWI, could profit from selective excitation, there currently is only a corresponding version of the former implemented on our systems.

As one of the most important components of mpMRI of the prostate, optimal image quality of the DWI sequence is crucial, and technologies reducing artifacts are desirable. Both rs-DWI and reduced-FOV sTX-DWI have been shown to improve DWI quality in pelvic applications compared to ss-DWI.[15,18,19] However, a direct comparison between these techniques in prostate MRI has not been performed yet to the best of our knowledge. A direct comparison between rs-DWI and sTX-DWI seems to be of interest also in view of the fact that the acquisition time using sTX-DWI can be accelerated substantially compared to rs-DWI.

Thus, the purpose of this study was to compare image quality and geometric distortion between rs-DWI and sTX-DWI of the prostate.

MATERIALS AND METHODS

This prospective multicenter study was approved by our regional ethics committee, and written informed consent was attained from all patients before the scan. The study was compliant with the Health Insurance Portability and Accountability Act.

Patients

Patients undergoing clinically indicated mpMRI of the prostate at 3 T between April and November 2014 at 2 radiologic institutions were eligible for the study (n = 102; median age, 64.2 years; range,

Received for publication February 12, 2015; and accepted for publication, after revision, May 11, 2015.

From the *Institute of Diagnostic and Interventional Radiology, University Hospital Zürich, Zurich; †Department for Radiology, Cantonal Hospital Aarau, Aarau; and ‡Department of Urology, University Hospital Zürich, Zurich, Switzerland.

Conflicts of interest and sources of funding: none declared.

Correspondence to: Olivio F. Donati, MD, Institute of Diagnostic and Interventional Radiology, University Hospital Zürich, Rämistrasse 100, CH-8091 Zürich, Switzerland. E-mail: olivio.donati@usz.ch.

ISSN: 0020-9996/15/0000–0000
DOI: 10.1097/RLI.0000000000000184

42.2–80.9 years). Patients were referred mainly because of elevated prostate-specific antigen (median, 6.28 μg/L; range, 1.0–1841.0 μg/L) and/or clinical suspicion for prostate cancer on digital rectal examination. Patients who underwent prostate mpMRI without an ERC (n = 22), who underwent prior surgical and/or radiation treatment (ie, radical prostatectomy, focal ablation, external beam therapy, and brachytherapy) of the prostate (n = 13) or who had incomplete acquisition (n = 2) were excluded. The final study population consisted of 65 patients (median age, 64.5 years; range 42.2–80.9 years) of whom 46 patients were recruited in the first institution (median age, 63.7 years; range, 48.1–80.9 years) and 19 patients in the second institution (median age, 51.0 years; range, 42.2–68.3 years). All patients underwent mpMRI of the prostate on a 3-T scanner including rs-DWI and reduced-FOV sTX-DWI.

MRI Technique

Images were acquired on 3-T whole body MRI systems (Magnetom Skyra, Siemens Healthcare, Erlangen, Germany) equipped with 2 independent transmit channels (TimTX TrueShape, Siemens Healthcare) in both participating institutions. An 18-channel phased-array receiver coil and a balloon-covered expandable endorectal coil (ERC; Medrad, Warrendale, Pa) were used for signal reception. No antiperistaltic drugs were applied.

Transverse T2-weighted turbo-spin echo images (TSE-T2w) were acquired with repetition time (TR)/ echo time (TE) typically, 3500/97 ms; FOV, 180 × 120 mm^2; slice thickness (ST), 3 mm; in-plane resolution, 0.2 × 0.2 mm^2.

Both DWI series were acquired in the transverse plane with identical orientation and at identical locations as the TSE-T2w images. The rs-DWI acquisition parameters were TR/minimum TE typically, 5400 /69 ms; receive bandwidth, 700 Hz/Px; *b* values, 0, 50, and 1000 seconds/mm^2; FOV, 150 × 150 mm^2; ST, 3 mm; in-plane resolution, 1.3 × 1.3 mm^2; read-out segments, 9; acquisition time, 8:18 minutes. The sTX-DWI acquisition parameters were: TR/minimum TE typically, 5700/94 ms (due to longer excitation pulse duration); receive bandwidth, 755 Hz/Px; *b* values, 0, 50, 1000 seconds/mm^2; reduced FOV, 77 × 150 mm^2; ST, 3 mm; in-plane resolution, 1.3 × 1.3 mm^2; acquisition time, 1:37 minutes. Apparent diffusion coefficient (ADC) maps were calculated on the scanner using a monoexponential fit based on the 3 obtained *b* values. The sequence parameters are summarized in Table 1.

Coronal and sagittal TSE-T2w images, transverse T1-weighted turbo-spin echo images and dynamic contrast-enhanced images were additionally obtained during the routine prostate protocol but not used for study purposes.

TABLE 1. Diffusion Sequence Parameters

	rs-DWI*	sTX-DWI†
b-value, s/mm^2	0, 50, 1000	0, 50, 1000
No. averages	1, 1, 2	1, 1, 4
Typical TR, ms	5400	5700
Minimum TE, ms	69	94
Matrix	112 × 112	59 × 112
Field of view, mm^2	150 × 150	77 × 150
In-plane resolution, mm	1.3 × 1.3	1.3 × 1.3
Number of sections	20	20
Section thickness, mm	3	3
Pixel bandwidth, Hz/px	700	755
Acquisition time	08:18	01:37

*Readout-segmented diffusion-weighted image.

†Selective-excitation accelerated diffusion-weighted image with reduced FOV.

Qualitative Image Analysis

Two radiologists (O.F.D., with 3 years of experience in interpreting prostate MRI, and B.K.B., a body imaging research fellow with 1 year of experience in interpreting prostate MRI) independently reviewed *b*-1000 images and corresponding ADC maps from both DWI sequences in 2 separate reading sessions (time interval between sessions, 2 weeks). The image sets were anonymized, and the anatomical region presented on screen was limited as required to assure blinding to the type of DWI sequence. The following image features were assessed on a 5-point Likert scale (1, poor; 2, below average; 3, average; 4, above average; 5, excellent): resolution (defined as the ability to identify anatomical details within the prostate), capsule demarcation (defined as the ability to continuously identify the prostatic capsule), zonal anatomy [defined as the ability to differentiate peripheral zone (PZ) from transition zone (TZ)] and overall image quality. Geometric distortion was graded visually for each DWI image series using a 5-point Likert scale (1, no distortion; 2, low distortion; 3, intermediate distortion; 4, high distortion; 5, very high distortion). Readers were allowed to fuse DWI and/or ADC images with TSE-T2w images to compare apparent geometric distortion. In addition, the presence of artifacts (ghosting and susceptibility) and the grade of their influence on image quality were noted (1, none; 2, low; 3, moderate; 4, severe; 5, substantial).

At the end of the second reading session, readers were presented a side-by-side display of ADC maps and *b*-1000 images from both DWI acquisitions and selected their overall preference.

Quantitative Image Analysis

After qualitative image analysis, one radiologist (B.K.B.) blinded to the type of DWI sequence used placed an elliptic region-of-interest (ROI) within healthy-appearing tissue in the PZ and TZ on the *b*-1000 image sets and ADC maps for each patient.[18] The mean size of the ROI in the PZ and TZ was 0.20 cm^2 ± 0.01 and 2.03 cm^2 ± 0.06, respectively. For estimation of signal-to-noise-ratio (SNR), a third ROI (nROI), with a mean size of 0.20 cm^2 ± 0.01, was placed on *b*-1000 images over an area containing barium sulfate within the ERC. All ROIs were placed carefully, avoiding focal lesions or artifacts. To ensure accurate matching, the ROIs were copied and pasted to the corresponding anatomic regions between DWI and ADC maps. The SNR was estimated as the ratio of mean signal intensity of the ROI in the PZ and TZ on b-1000 image sets, respectively, and the standard deviation (SD) of the nROI.[20,21] Mean ADC values and SD of each ROI in the PZ and TZ were recorded. Both the estimated mean SNR and mean ADC values of each ROI in the PZ and TZ, respectively, were averaged to obtain a single value for the whole prostate.

For quantification of geometric distortion, diameters in the anteroposterior (AP) and left-right (LR) direction on transverse images of the prostate were measured on the level of the verumontanum on b-1000 image sets of both DWIs and the TSE-T2w. The latter served as the standard of reference regarding anatomic borders. Differences in diameters between both DWI sequences and TSE-T2w were calculated. The quantitative analysis was performed using a free DICOM viewer (Osirix, version 5.9; The OsiriX Foundation, Geneva, Switzerland).

Statistical Analysis

Continuous variables were summarized by using mean and standard deviation (SD) values or medians and ranges. Categorical variables were summarized as counts and proportions. The Kolmogorov-Smirnov test was used to assess the distribution of data. Intersequence comparison of qualitative parameters, SNR, ADC values, and prostate diameter was performed using a Wilcoxon matched pair test when data were not normally distributed or a paired *t* test when a normal distribution was

TABLE 2. Comparison of Qualitative Scores for Image Features, Overall Image Quality and Geometric Distortion Between rs-DWI and sTX-DWI, as Assessed by Readers 1 and 2 and Inter-Reader Agreement for rs-DWI and sTX-DWI Qualitative Scores are expressed as mean ± SD on a 5-point Likert Scale

	Reader 1			Reader 2			Inter-Reader Agreement	
Scores	**rs-DWI***	**sTX-DWI†**	***P*‡**	**rs-DWI***	**sTX-DWI†**	***P*‡**	**ICC‡ (rs-DWI)**	**ICC‡ (sTX-DWI)**
Resolution	3.95 ± 0.65	3.75 ± 0.94	0.144	4.17 ± 0.73	4.02 ± 0.73	0.111	0.59 [0.40, 0.73]	0.63 [0.45, 0.76]
Capsule demarcation	4.12 ± 0.63	4.17 ± 0.07	0.577	4.22 ± 0.72	4.20 ± 0.69	0.866	0.42 [0.20, 0.60]	0.48 [0.27, 0.65]
Zonal anatomy	3.71 ± 0.84	3.75 ± 0.94	0.577	3.48 ± 0.89	3.62 ± 0.84	0.095	0.59 [0.40, 0.73]	0.65 [0.48, 0.77]
Overall image quality	4.09 ± 0.66	4.03 ± 0.79	0.433	3.86 ± 0.66	3.80 ± 0.74	0.465	0.50 [0.30, 0.66]	0.69 [0.53, 0.80]
Geometric distortion	1.74 ± 0.67	2.17 ± 0.84	**<0.001**	1.55 ± 0.64	2.09 ± 0.95	**<0.001**	0.49 [0.28, 0.66]	0.74 [0.61, 0.83]
Influence of artifact on image quality	2.02 ± 0.63	2.43 ± 0.70	**<0.001**	2.16 ± 0.73	2.60 ± 0.77	**<0.05**	0.49 [0.25, 0.68]	0.64 [0.43, 0.79]

Likert scale used for parameters "resolution, capsule demarcation, zonal anatomy, and overall image quality": 1, poor; 2, below average; 3, average; 4, above average; 5, excellent.

Likert scale used for parameter "geometric distortion": 1, no distortion; 2, low distortion; 3, intermediate distortion; 4, high distortion; 5, very high distortion).

Likert scale used for parameter "influence of artifact on image quality": 1, none; 2, low; 3, moderate; 4, severe; 5, substantial).

Interclass correlation coefficients (ICC) are expressed with 95% CI.

*Readout-segmented diffusion-weighted image.

†Selective-excitation accelerated diffusion-weighted image with reduced FOV.

‡Listed in bold when statistically significant at $P < 0.05$.

found. The level of inter-rater agreement for each assessed qualitative parameter and quantitative degree of geometric distortion was measured by the intraclass correlation coefficient (ICC, 2-way random), including 95% confidence intervals (CIs). $P < 0.05$ was considered statistically significant. Statistical analysis was performed with IBM SPSS statistical software (SPSS version 21; Chicago, Ill).

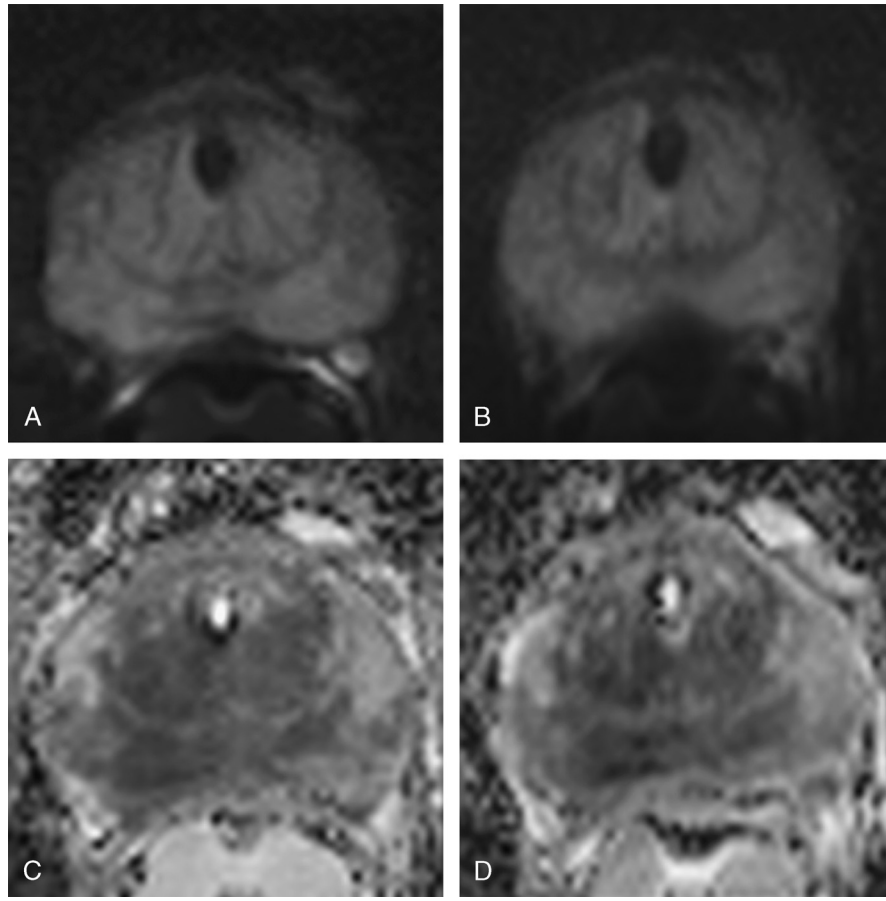

FIGURE 1. A 60-year-old male patient undergoing mpMRI of the prostate. Rs-DWI b-1000 slice (A), reduced-FOV sTX-DWI *b*-1000 slice (B), rs-DWI ADC map (C), and reduced-FOV sTX-DWI ADC map (D) are shown. Both sequences (including ADC maps) were rated above average by reader 1 and excellent by reader 2 in overall image quality.

RESULTS

Qualitative Analysis

There was no significant difference in resolution, capsule demarcation, zonal anatomy, and overall image quality between rs-DWI and sTX-DWI for either reader (Table 2). Overall image quality was rated "above average" by reader 1 (4.09 ± 0.66 and 4.03 ± 0.79) and reader 2 (3.86 ± 0.66 and 3.80 ± 0.74) for rs-DWI and sTX-DWI, respectively (Fig. 1, Table 2). Differences between rs-DWI and sTX-DWI were not statistically significant for either reader ($P = 0.433$ for reader 1 and $P = 0.465$ for reader 2).

Although altogether low, both readers rated the level of geometric distortion lower for rs-DWI than for sTX-DWI (reader 1, 1.74 ± 0.67 and 2.17 ± 0.84; $P < 0.001$; reader 2, 1.55 ± 0.64 and 2.09 ± 0.95; $P < 0.001$) (Fig. 2, Table 2). Overall, artifacts on rs-DWI and sTX-DWI had only low impact on image quality (2.04 ± 0.62 and 2.43 ± 0.70 for reader 1; 2.18 ± 0.76 and 2.64 ± 0.74 for reader 2) (Fig. 3). Impact on image quality was higher for sTX-DWI than rs-DWI according to both readers ($P < 0.001$ for reader 1 and $P < 0.05$ for reader 2). Artifact frequencies, as assessed by readers 1 and 2, are shown in Table 3.

Inter-reader agreement ranged between 0.42 and 0.74 for all assessed features including resolution [ICC, 0.59 (95% CI, 0.40–0.73) and 0.63 (95% CI, 0.45–0.76)], overall image quality [ICC, 0.50 (95% CI, 0.30–0.66) and 0.69 (95% CI, 0.53–0.80)], geometric distortion [ICC, 0.49 (95% CI, 0.28–0.66) and 0.74 (95% CI, 0.61–0.83)] and influence of artifact on image quality [ICC, 0.49 (95% CI, 0.25–0.68) and 0.64 (95% CI, 0.43–0.79)], for rs-DWI and sTX-DWI, respectively. On a side-by-side comparison, reader 1 preferred rs-DWI over sTX-DWI in 60% and reader 2 in 55.4% of cases.

Quantitative Analysis

The results of the quantitative analysis are shown in Table 4.

The SNR was slightly lower for rs-DWI compared to sTX-DWI in the whole gland [(38.56 ± 15.25) and (41.63 ± 15.80); $P < 0.05$] as well as in the TZ [(35.81 ± 14.71) and (39.32 ± 14.86); $P < 0.05$]. The SNR in the PZ was not significantly different between rs-DWI and sTX-DWI [(41.30 ± 16.91) and (43.93 ± 17.69); $P = 0.144$]. Mean ADC value was slightly but significantly lower for rs-DWI compared to sTX-DWI in the PZ [$(1.77 \times 10^{-3}$ mm^2/s ± 0.26) and $(1.84 \times 10^{-3}$ mm^2/s ± 0.28); $P < 0.001$], whereas there was no significant difference in the TZ [$(1.45 \times 10^{-3}$ mm^2/s ± 0.21) and $(1.45 \times 10^{-3}$ mm^2/s ± 0.13); $P = 0.583$] or regarding the whole gland [$(1.61 \times 10^{-3}$ mm^2/s ±0.16) and $(1.64 \times 10^{-3}$ mm^2/s ±0.18); $P = 0.111$].

The mean prostate AP diameter was measured larger on DWI images than on TSE-T2w images with mean diameter differences of 0.9 mm ± 2.2 for rs-DWI and 2.1 mm ± 3.8 for sTX-DWI ($P < 0.001$). Differences in mean LR diameter were not significant between TSE-T2w and rs-DWI (−0.4 mm ± 1.8; $P = 0.055$) or sTX-DWI (−0.4 mm ± 2.3; $P = 0.123$). Anteroposterior diameters measured on rs-DWI showed significantly higher agreement with TSE-T2w [ICC, 0.96 (95% CI, 0.94–0.96)] than sTX-DWI [ICC, 0.89 (95% CI, 0.83–0.93)] as suggested by the nonoverlapping CIs. There was no

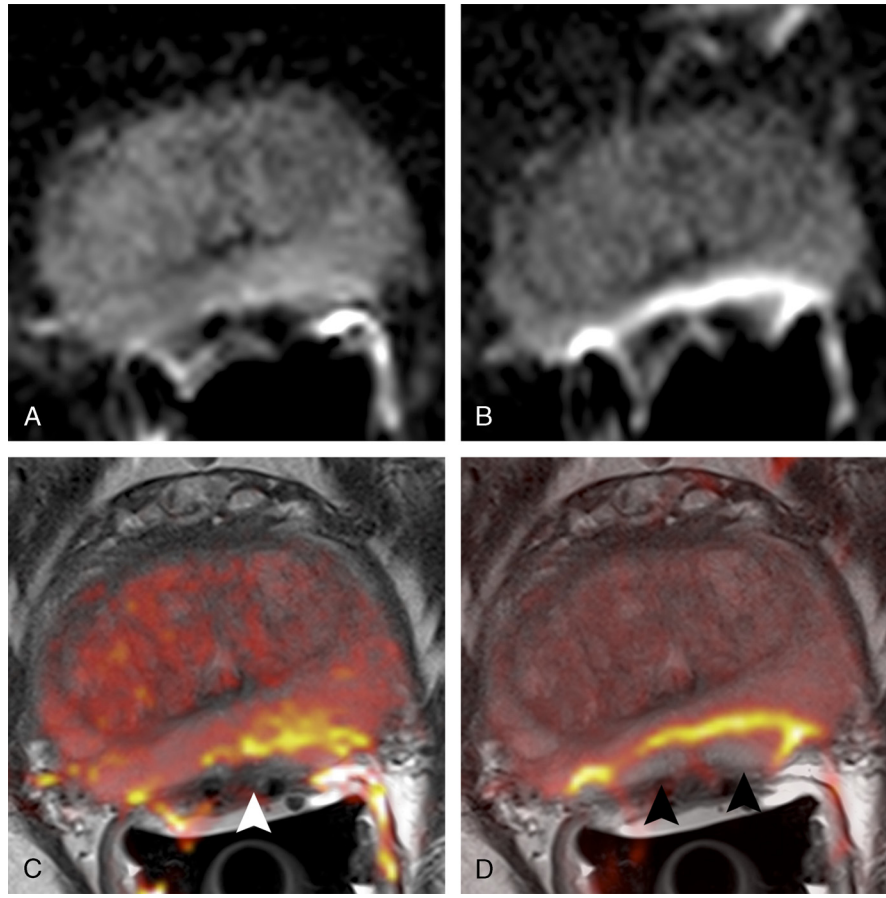

FIGURE 2. A 58-year-old male patient undergoing mpMRI of the prostate. Rs-DWI b-1000 image (A), reduced-FOV sTX-DWI b-1000 image (B), TSE-T2w image fused with rs-DWI b-1000 image (C), and with reduced-FOV sTX-DWI b-1000 image (D) at the level of the midgland are shown. The geometric distortion at the posterior aspect of the prostate close to the rectum-prostate border (arrowheads) is more pronounced on sTX-DWI (images B and D) than on rs-DWI (images A and C). Figure 2 can be viewed online in color at www.investigativeradiology.com.

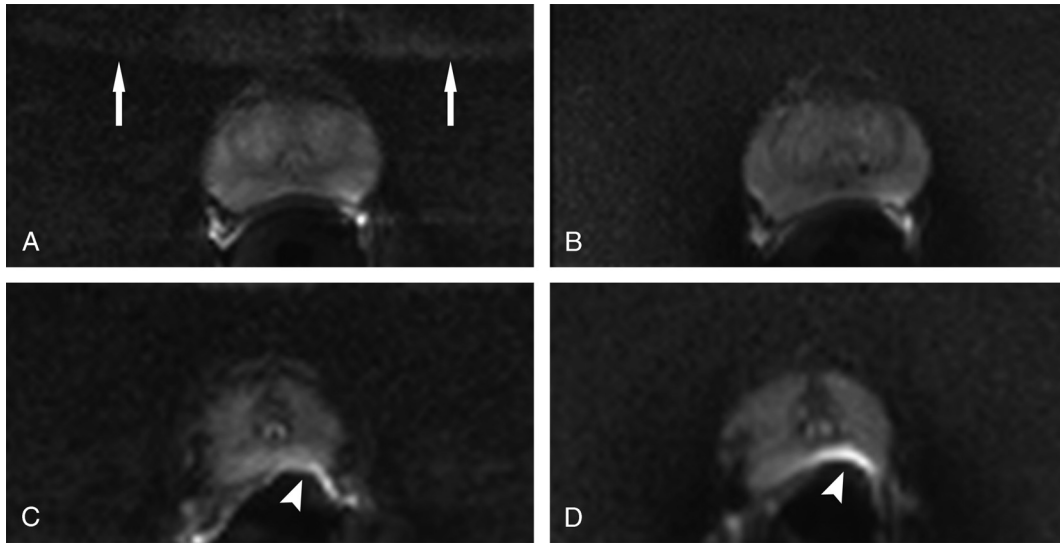

FIGURE 3. A 68-year-old male patient undergoing mpMRI of the prostate. Ghosting artifact (arrows) is present on rs-DWI b-1000 image (A) but not on reduced-FOV sTX-DWI b-1000 image (B) of the same patient at the level of the midgland. Susceptibility artifacts (arrowheads) are less pronounced on rs-DWI b-1000 image (C) than on reduced-FOV sTX-DWI b-1000 image (D) in the same patient at the level of the apex.

significant difference in agreement with TSE-T2w for measurements of the LR diameter [ICC, 0.98 (95% CI, 0.96–0.98]) and [ICC, 0.96 (95% CI, 0.94–0.98]) for rs-DWI and sTX-DWI, respectively.

DISCUSSION

Diffusion-weighted imaging is an important component of mpMRI of the prostate, improving detection and localization of prostate cancer,[7] which provides essential information on cancer aggressiveness[5,6] and may allow estimating volume of prostate cancer foci.[4,22] Thus, in clinical practice, DWI sequences that are robust, render high-quality images of the prostate and which can be acquired within a reasonable time are crucial. Our analysis of 2 newly introduced techniques of DWI applied in prostate MRI, rs-DWI, and selective-excitation accelerated reduced-FOV sTX-DWI, suggests comparable image quality.

Readout-segmented DWI has been shown to be a promising technique for high-resolution DWI in the brain,[12–14] the abdomen,[15,23] and the breast,[24] causing less geometric distortion than traditional ss-DWI. Another DWI technique leading to a reduction of artifacts related to high-field inhomogeneity is selective-excitation technology (sTX), commercially enabled by a parallel-transmit system.[17] Two studies have compared reduced-FOV sTX-DWI to ss-DWI in the prostate.[18,19] Rosenkrantz et al[18] demonstrated superior image quality of sTX-DWI compared to ss-DWI acquired with standard excitation. The improvements in image quality of sTX-DWI were most apparent in images in which a small FOV (14 cm^2) similarly to ours was used. Thierfelder et al[19] also showed improvement of image quality for sTX-DWI compared to standard conventional DWI. Whereas the sTX-DWI sequence in their study was acquired in 4:21 minutes and compared to a ss-DWI acquired in 2:43 minutes, acquisition time of the sTX-DWI sequence in our study was only 1:37 minutes. Despite the more than 5-fold decrease in acquisition time, reduced-FOV sTX-DWI was comparable to rs-DWI regarding image quality parameters. However, when readers had to decide between the 2 DWI sequences in a side-by-side presentation, they favored the image quality rendered by the rs-DWI in 55% and 60% of the cases, respectively. This might be due to the more pronounced geometric distortion and susceptibility artifacts of the sTX-DWI sequence compared to rs-DWI. These artifacts are mainly caused by inhomogeneities of the static magnetic field (B0), caused by air in the rectum or within the endorectal coil (ERC) near the prostate.[25] Without the use of an ERC, these artifacts may also be present especially if the rectum is not voided before the examination and there is air remaining in the rectum at the rectoprostatic border. In setting up the 2 DWI-sequences for direct comparison, we focused on keeping major sequence parameters such as in-plane resolution, ST, TR, TE, *b* values, and also the bandwidth as close as possible while targeting similar SNRs for a fair comparison. Indeed, rather comparable SNR values could be achieved (compare Table 4), with the main reason of the minimally higher SNR in the sTX-DWI images likely being the increased number of averages. The relatively low bandwidth chosen to

TABLE 3. Frequencies of Artifacts for rs-DWI and sTX-DWI, as Assessed by Readers 1 and 2

	Reader 1		Reader 2		Overall (Pooled Data)	
	rs-DWI*	sTX-DWI†	rs-DWI*	sTX-DWI†	rs-DWI*	sTX-DWI†
Artifact						
Ghosting	26 (43.3)	4 (7.4)	36 (53.7)	8 (16.7)	62 (48.2)	12 (11.8)
Susceptibility	34 (56.7)	50 (92.6)	31 (46.3)	40 (83.3)	65 (51.2)	90 (88.2)
Total	60 (100)	54 (100)	67 (100)	48 (100)	127 (100)	102 (100)

Frequency distribution expressed in absolute and relative counts (%) in a data set consisting of 65 patients.

*Readout-segmented diffusion-weighted image.

†Selective-excitation accelerated diffusion-weighted image with reduced FOV.

TABLE 4. Quantitative Analysis of SNR and ADC Values Between rs-DWI and sTX-DWI

	rs-DWI*	sTX-DWI†	P‡
SNR§			
Peripheral zone	41.30 ± 16.91	43.93 ± 17.69	0.144
Transitional zone	35.81 ± 15.80	39.32 ± 14.86	**<0.05**
Total SNR	38.56 ± 15.25	41.63 ± 15.80	**<0.05**
ADC‖			
Peripheral zone	1.70 ± 0.26	1.84 ± 0.28	**<0.001**
Transitional zone	1.45 ± 0.21	1.45 ± 0.13	0.583
Total ADC	1.61 ± 0.16	1.64 ± 0.18	0.111

Signal-to-noise-ratio and ADC are expressed as mean ± standard deviation (SD).

*Readout-segmented DWI.

†Selective-excitation accelerated diffusion-weighted image with reduced FOV.

‡Listed in bold when statistically significant at $P < 0.05$.

§Signal-to-noise ratio.

‖Apparent diffusion coefficient [unit: $\times 10^{-3}$ mm^2/s].

keep parameters comparable between the 2 DWI sequences did cause relatively long echo train durations in the sTX-DWI sequences, therefore increasing susceptibility artifacts and geometric distortion. By increasing the bandwidth in sTX-DWI theses, artifacts may be decreased at the expense of a lower SNR and/or a longer acquisition time.

Both DWI sequences demonstrated above average image quality regarding resolution, demarcation of the prostatic capsule, differentiation of zonal anatomy, and overall image quality with only nonsignificantly higher scores using rs-DWI. The minimally higher SNR of the prostate on sTX-DWI compared to rs-DWI was probably due to the number of averages for the *b* value of 1000 seconds/mm^2, which was 4 for the sTX versus 2 for the rs-DWI. This value was chosen to achieve comparable SNR between the sequences while maintaining the marked decrease in acquisition time of sTX-DWI.

The comparison of ADC values between DWI sequences evidenced higher values for sTX-DWI than for rs-DWI in the PZ, whereas there were no significant differences regarding the TZ or the whole gland. We hypothesize that in part, this may be attributed to the longer TE in the sTX-DWI sequence, which may have resulted in a stronger attenuation of microperfusion-associated signal components at low *b* values. Apparent diffusion coefficient values have been shown to depend on different factors including field strength, coil system, vendors, gradient performance, respiratory compensation technique, TR, TE, choice, and number of *b* values,[22,26–29] values which have been kept constant between the 2 sequences in our study. The reason for the difference in ADC in the PZ of the prostate remains unproven, however such differences between sTX-DWI and standard sinc pulse DWI have been shown before.[18]

Artifacts caused by the DWI sequences had a low impact on image quality. While ghosting artifacts were more frequently present in rs-DWI, susceptibility artifacts were more frequent in sTX-DWI. Whereas the latter can be explained by the relatively low bandwidth chosen in sTX-DWI for reasons of comparability of sequence parameters, the ghosting artifacts on rs-DWI can be explained by the segmented filling of k-space data in temporally separated steps and in the presence of—although—small displacements of imaged anatomy in combination with the relatively long acquisition time.

We acknowledge the following limitations: First, since the study was not designed to address the issue of diagnostic accuracy, and hence no histopathologic matching was done, lesion- or condition-specific qualitative parameters (ie, lesion conspicuity) were not evaluated. However, the presence of these conditions may have altered the impression of overall image quality. Second, the time invested in acquisition of rs-DWI was 5 times longer than the time invested for sTX-DWI. However, our goal was to keep the 2 DWI sequences as similar as possible in parameters such as in-plane resolution, ST, TR, TE, receive bandwidth, and SNR. It may be hypothesized that by increasing the bandwidth for the sTX-DWI, geometric distortion and susceptibility artifacts would be less pronounced and SNR could be improved by increasing the number of averages in high *b*-value images while still keeping the acquisition time significantly shorter than in rs-DWI.

In summary, we demonstrated that diffusion-weighted images of the prostate acquired with a reduced field of view enabled by selective excitation in a more than 5-fold shorter acquisition time were of comparable image quality as those acquired with a readout-segmented sequence. The increase in geometric distortion, mostly due to the low bandwidth chosen for sequence comparison, did not affect image quality to a large extent.

REFERENCES

1. Barentsz JO, Richenberg J, Clements R, et al. ESUR prostate MR guidelines 2012. *Eur Radiol*. 2012;22:746–757.
2. Baur AD, Maxeiner A, Franiel T, et al. Evaluation of the prostate imaging reporting and data system for the detection of prostate cancer by the results of targeted biopsy of the prostate. *Invest Radiol*. 2014;49:411–420.
3. Maas MC, Futterer JJ, Scheenen TW. Quantitative evaluation of computed high B value diffusion-weighted magnetic resonance imaging of the prostate. *Invest Radiol*. 2013;48:779–786.
4. Donati OF, Afaq A, Vargas HA, et al. Prostate MRI: evaluating tumor volume and apparent diffusion coefficient as surrogate biomarkers for predicting tumor Gleason score. *Clin Cancer Res*. 2014;20:3705–3711.
5. Donati OF, Mazaheri Y, Afaq A, et al. Prostate cancer aggressiveness: assessment with whole-lesion histogram analysis of the apparent diffusion coefficient. *Radiology*. 2014;271:143–152.
6. Hambrock T, Somford DM, Huisman HJ, et al. Relationship between apparent diffusion coefficients at 3.0-T MR imaging and Gleason grade in peripheral zone prostate cancer. *Radiology*. 2011;259:453–461.
7. Vargas HA, Akin O, Franiel T, et al. Diffusion-weighted endorectal MR imaging at 3 T for prostate cancer: tumor detection and assessment of aggressiveness. *Radiology*. 2011;259:775–784.
8. Selnaes KM, Heerschap A, Jensen LR, et al. Peripheral zone prostate cancer localization by multiparametric magnetic resonance at 3 T: unbiased cancer identification by matching to histopathology. *Invest Radiol*. 2012;47:624–633.
9. Somford DM, Hambrock T, Hulsbergen-van de Kaa CA, et al. Initial experience with identifying high-grade prostate cancer using diffusion-weighted MR imaging (DWI) in patients with a Gleason score ≤ 3 + 3 = 6 upon schematic TRUS-guided biopsy: a radical prostatectomy correlated series. *Invest Radiol*. 2012;47:153–158.
10. Lee VS, Hecht EM, Taouli B, et al. Body and cardiovascular MR imaging at 3.0 T. *Radiology*. 2007;244:692–705.
11. Porter DA, Heidemann RM. High resolution diffusion-weighted imaging using readout-segmented echo-planar imaging, parallel imaging and a two-dimensional navigator-based reacquisition. *Magn Reson Med*. 2009;62:468–475.
12. Holdsworth SJ, Yeom K, Skare S, et al. Clinical application of readout-segmented-echo-planar imaging for diffusion-weighted imaging in pediatric brain. *AJNR Am J Neuroradiol*. 2011;32:1274–1279.
13. Morelli J, Porter D, Ai F, et al. Clinical evaluation of single-shot and readout-segmented diffusion-weighted imaging in stroke patients at 3 T. *Acta Radiol*. 2013;54:299–306.
14. Yeom KW, Holdsworth SJ, Van AT, et al. Comparison of readout-segmented echo-planar imaging (EPI) and single-shot EPI in clinical application of diffusion-weighted imaging of the pediatric brain. *AJR Am J Roentgenol*. 2013;200:W437–W443.
15. Thian YL, Xie W, Porter DA, et al. Readout-segmented echo-planar imaging for diffusion-weighted imaging in the pelvis at 3 T—A feasibility study. *Acad Radiol*. 2014;21:531–537.
16. Holdsworth SJ, Skare S, Newbould RD, et al. Readout-segmented EPI for rapid high resolution diffusion imaging at 3 T. *Eur J Radiol*. 2008;65:36–46.
17. Blasche M, Riffel P, Lichy M. TimTX TrueShape and syngo ZOOMit Technical and Practical Aspects. *Magnetom Flash*. 2012:74–84.
18. Rosenkrantz AB, Chandarana H, Pfeuffer J, et al. Zoomed echo-planar imaging using parallel transmission: impact on image quality of diffusion-weighted imaging of the prostate at 3 T. *Abdom Imaging*. 2015;40:120–126.
19. Thierfelder KM, Scherr MK, Notohamiprodjo M, et al. Diffusion-weighted MRI of the prostate: advantages of zoomed EPI with parallel-transmit–accelerated 2D-selective excitation imaging. *Eur Radiol*. 2014;24:3233–3241.

20. Heverhagen JT. Noise measurement and estimation in MR imaging experiments. *Radiology*. 2007;245:638–639.
21. Kaufman L, Kramer DM, Crooks LE, et al. Measuring signal-to-noise ratios in MR imaging. *Radiology*. 1989;173:265–267.
22. Mazaheri Y, Vargas HA, Nyman G, et al. Image artifacts on prostate diffusion-weighted magnetic resonance imaging: trade-offs at 1.5 Tesla and 3.0 Tesla. *Acad Radiol*. 2013;20:1041–1047.
23. Tokoro H, Fujinaga Y, Ohya A, et al. Usefulness of free-breathing readout-segmented echo-planar imaging (RESOLVE) for detection of malignant liver tumors: comparison with single-shot echo-planar imaging (SS-EPI). *Eur J Radiol*. 2014;83:1728–1733.
24. Wisner DJ, Rogers N, Deshpande VS, et al. High-resolution diffusion-weighted imaging for the separation of benign from malignant BI-RADS 4/5 lesions found on breast MRI at 3 T. *J Magn Reson Imaging*. 2014;40:674–681.
25. Rosen Y, Bloch BN, Lenkinski RE, et al. 3 T MR of the prostate: reducing susceptibility gradients by inflating the endorectal coil with a barium sulfate suspension. *Magn Reson Med*. 2007;57:898–904.
26. Donati OF, Chong D, Nanz D, et al. Diffusion-weighted MR imaging of upper abdominal organs: field strength and intervendor variability of apparent diffusion coefficients. *Radiology*. 2014;270:454–463.
27. Kwee TC, Takahara T, Koh DM, et al. Comparison and reproducibility of ADC measurements in breathhold, respiratory triggered, and free-breathing diffusion-weighted MR imaging of the liver. *J Magn Reson Imaging*. 2008;28:1141–1148.
28. Padhani AR, Liu G, Koh DM, et al. Diffusion-weighted magnetic resonance imaging as a cancer biomarker: consensus and recommendations. *Neoplasia*. 2009;11:102–125.
29. Sasaki M, Yamada K, Watanabe Y, et al. Variability in absolute apparent diffusion coefficient values across different platforms may be substantial: a multivendor, multi-institutional comparison study. *Radiology*. 2008;249:624–630.